# Microstructure of Ca−AOT/Water/Decane w/o Microemulsions

**Francesca Caboi,[†] Giulia Capuzzi,[‡] Piero Baglioni,[‡] and Maura Monduzzi*[,†]**

*Dipartimento Scienze Chimiche, Universita' di Cagliari, Via Ospedale 72, 09124 Cagliari, Italy, and Dipartimento di Chimica, Universita' di Firenze, Via G. Capponi 9, 50121 Firenze, Italy*

*Received: April 14, 1997; In Final Form: September 6, 1997*[⊗]

The microstructural features of the ternary microemulsion CaAOT/water/*n*-decane are investigated by viscosity, conductivity, dynamic light scattering, and NMR self-diffusion measurements. The phase diagram shows a significant shrinkage of the microemulsion region, compared with the corresponding NaAOT system, which implies a decrease of the capability of water uptake. This is also observed for the $L_\alpha$ phase of the binary CaAOT/water system. A preliminary analysis of viscosity data suggests the occurrence of nonspherical particles at high volume fraction of the disperse phase, $\phi_d$, whereas the conductivity measurements show a percolative behavior at a critical $\phi_d^c = 0.142$, along an oil dilution line at constant molar ratio w/s = 26.4. The percolation threshold is not temperature dependent in the range 15−30 °C, thus suggesting the possibility of a static percolation. The comparison between the diffusion coefficients calculated from composition and those obtained by DLS and NMR measurements reveals that spherical droplets with a hard-sphere behavior are likely to occur in a very limited region of the $L_2$ phase, namely, at low $\phi_d$. The conductivity measurements and the NMR self-diffusion coefficients of water, measured along several water dilution lines, display significant maxima, appearing at $w°$ ($[H_2O]/2[CaAOT]$) between 6 and 13 (conductivity, diffusion, and $w°$ values, at the maximum, increase with increasing the s/o ratio), in evident conflict with a hard-sphere model. All experimental data demonstrate the occurrence of important modifications of the water-in-oil droplet organization. The microstructure of the system is discussed in view of different approaches based on percolation theory, attractive interactions among discrete particles, and multiconnected water network. Microstructural evolutions can be justified in terms of transient fusion−fission processes among the droplets occurring over time scales that are comparable with the experimental (conductivity and NMR) observation times. Similar results have been obtained by considering the geometrical DOC model set up to interpret the transition from a bicontinuous to a water-in-oil droplet microstructure in DDAB microemulsions.

## Introduction

The microemulsions formed by the anionic surfactant sodium bis(2-ethylhexyl) sulfosuccinate (AOT) have been widely investigated as model systems since water-in-oil (w/o) microemulsions ($L_2$ phase) are easily obtained without a cosurfactant,[1−4] and are thermodynamically stable over a wide range of temperature and composition. A great deal of knowledge, concerning the microstructure, the droplet size, the polydispersity, and the static and dynamic percolation phenomena, is actually available from many different techniques.[5−22]

Although many detailed investigations, which are summarized in some interesting review articles,[3,4,23,24] the AOT surfactant is still a topical subject, as demonstred by several recent papers which are still dealing with microstructural characterizations.[25−33] Most studies pointed out that microstructure of AOT w/o microemulsions is reasonably well described in terms of spherical droplets,[34] although various experiments, carried out as a function of several parameters such as surfactant concentration, temperature, type of oil and following different dilution criteria, provided evidence of anomalous behavior with respect to a hard-sphere system. So far, discrepancies have been discussed within a context of critical phenomena, microstructural transitions and percolation theory.[26,30,32,35] From literature data, it appears firmly established that hard sphere particles, characterized by Brownian diffusion-controlled motions, are allowed in the diluted region only, at a volume fraction of the dispersed phase $\phi_d = \phi_w + \phi_s < 0.1$ (subscripts w and s refer to water and surfactant, respectively), i.e., close to the oil corner. With increasing $\phi_d$ there is strong evidence for the existence of short-range attractive interactions, which are oil and temperature dependent.[4] At high values of $\phi_d$, spherical droplets densely packed within a body-centered cubic lattice have been demonstrated by SANS measurements.[36] The attractive interactions prolong the lifetime of the particles' encounters and produce a cluster of droplets, thus generating water networks throughout the $L_2$ phase. This clustering, which is associated with changes of various macroscopic parameters, such as viscosity and electrical conductivity, can be understood in terms of "percolation".[30,33,37] Percolation occurs when the volume fraction $\phi_d$ reaches a critical value $\phi_d^c$ at constant temperature, when the temperature reaches a value $T_c$ at constant $\phi_d$ or when the water to surfactant (w/s) molar ratio increases. Due to this transition, conductivity can be represented by two separate asymptotic scaling power law with exponents that are different above and below the percolation threshold.[30,33,37]

The static percolation theory attributes this phenomenon to the appearance of bicontinuous microemulsions,[38] and the sharp increase of the conductivity can be explained by a connected water path in the system. Both counterions and, at a less extent, surfactant ions determine conductivity throughout the water network.[33] In the dynamic percolation model the attractive interdroplet interactions are responsible for the formation of percolative clusters,[39] and conductivity is mainly due to the motion of counterions along the water channels.[33] It has been suggested that below the static percolation threshold, dynamic

* To whom correspondence should be addressed. Tel. 39-70-6758604; Fax: 39-70-6758605; e-mail: monduzzi@vaxca1.unica.it.
[†] Universita' di Cagliari.
[‡] Universita' di Firenze.
[⊗] Abstract published in *Advance ACS Abstracts,* November 15, 1997.

S1089-5647(97)01274-1 CCC: $14.00 

percolation can also take place. In this case water channels can form when the surfactant interface, separating adjacent water cores, breakes down during collisions or through the transient merging of droplets. The observation of the phenomenological transitions of a system, in terms of static or dynamic percolation, can be strictly dependent on the time scale of the experimental technique. The kinetic constants which regulate the lifetime of the clustering interaction and thus the exchange of material, may range over a wide time scale.[7,40] For instance, it has been suggested that relaxation processes connected with percolation may be only described by a complex range of relaxation times, as evidentiated by a $^{13}C$ multifrequency NMR relaxation study.[17] Among the various techniques, conductivity has been shown to best satisfy the required time scale in most cases.

The microstructural transitions from bicontinuous to w/o closed domains, suggested by conductivity and NMR self-diffusion data, can be successfully described in terms of the geometrical DOC model.[41,42] The DOC model, the Disordered Open Connected model, consists of spheres which are connected to $Z$ nearest neighbors through cylinders: the number of connection for each sphere is strictly related to the dimension of the water domain. In the case of w/o microemulsions formed by the double-chained didodecyldimethylammonium bromide (DDAB) surfactant with several oils and also in the case of perfluoropolyether (PFPE) w/o microemulsions,[43,44] the use of the DOC model evidentiated a gradual transition of the microstructure from bicontinuity ($Z_{max} = 13.4$) to disconnected w/o droplets ($Z_{min} = 0$) along water dilution lines with increasing the water content.

The limit of most investigations concerning AOT w/o microemulsions is that experiments have been mainly performed as a function of temperature, and a restricted range of composition of the $L_2$ region (a dilution line or even a single point of the ternary phase diagram) has been examined thus providing an incomplete view of the microstructural evolutions occurring within the whole region.

In this work, the microemulsion region of the ternary system CaAOT/water/*n*-decane (CaAOT/W/C10) is investigated for the phase behavior in comparison with the AOT/W/C10,[13] with highlight on the effect of replacing the divalent $Ca^{2+}$ for the monovalent $Na^+$ counterion. It is well-known that electrostatic forces strongly affect the internal microstructure and the relative stability of different phases, as demonstrated by the addition of electrolyte salts to a surfactant system which can produce a Winsor I−Winsor II transition through a Winsor III bicontinuous microstructure.[45] Similarly, the charge of the counterion is expected to play a crucial role on the electrostatic interactions and the hydration strength. In the CaAOT/water binary system the main difference from the corresponding sodium AOT/water system consists of a significant reduction of the extension of the lamellar ($L_\alpha$) region.[46,47] The monophasic $L_\alpha$ phase occurs at about 65 wt % CaAOT only, whereas minor differences in the formation and range of existence of the bicontinuous cubic $V_2$ and of the reverse hexagonal $H_2$ phases are observed. These findings agree with theoretical Poisson−Boltzmann and Monte Carlo calculations which predict substantially smaller interlamellar repulsion with divalent than with monovalent counterions. This, in turns, decreases the capability of the $L_\alpha$ phase to swell and incorporate as much water as in the case of NaAOT.[48]

Few papers report on the w/o microemulsions formed by AOT with divalent counterions. A microemulsion CaAOT/W/cyclohexane at low $\phi_d$ ($\phi_d < 0.1$, and w/s = 10) was used to prepare spherical $CaCO_3$ particles.[49] The diluted regions of other microemulsions with the divalent counterions $Ca^{2+}$, $Mg^{2+}$, $Co^{2+}$, $Ni^{2+}$, $Cu^{2+}$, $Zn^{2+}$ and the cyclohexane oil were investigated at low water content by several techniques.[31,50−53] It has been shown by SAXS and SANS measurements that microemulsions formed by AOT with divalent counterions consist of w/o spherical droplets at low w/s, and ellipsoidal or cylindric particles at high w/s, with the exception of CaAOT for which a structural behavior similar to AOT was claimed.[50] Particularly in the case of Co−, Cu−, and CdAOT/W/isooctane microemulsions, a strong decrease of the water uptake together with transitions from a spherical shape of the droplets to interconnected cylinders, with increasing w/s, have been observed.[54]

It should be again remarked that for any of the investigated bimetallic−AOT microemulsion systems limited ranges of the $L_2$ microemulsion region were examined, and no phase diagram has been ever reported.

In this work, the whole range of the $L_2$ region is investigated by various and complementary techniques and by following different dilution criteria to map out the structural transitions and the variations of the interaction forces in relation with the phase diagram.

## Experimental Section

**Materials.** Bis(2-ethylhexyl) sodium sulfosuccinate (AOT) and *n*-decane (C10) were purchased from Sigma-Aldrich. The calcium salt of AOT was prepared by aqueous metathesis of a saturated solution of $Ca(NO_3)_2$ (Aldrich AR) with an ethanolic solution of NaAOT. The CaAOT precipitate was separated from the aqueous phase by centrifuge and washed repeatedly with Millipore filtered bi-distilled water (conductivity $< 10^{-6}$ S/m at 25 °C) until complete disappearance of $NO_3^-$ (determined by the brown ring test) and $Na^+$ (atomic adsorption spectroscopy) ions. The remaining water was eliminated by freeze-drying.

The microemulsion single-phase region of the ternary system was determined at 25 °C by diluting with water several samples at constant surfactant/oil (s/o) weight ratio.

**Viscosity.** The viscosity of the continuous phase was measured by an Ubbelhode viscosimeter with an accuracy of 1%. All the mesurements were performed at $T = 25 \pm 0.1$ °C.

**Conductivity.** The conductivity measurements were performed with a Hewlett-Packard 4192A Low-Frequency Impedance Analyzer, in the range from 5 Hz to 13 MHz (signal intensity 50 mV to 1 V, depending on the sample conductivity). The cell, temperature controlled within ± 0.1 °C by a thermostatic bath, was a four-terminal sample holder with parallel, rectangular gold plate electrodes with surfaces roughened to minimize electrode polarization.

**Dynamic Light Scattering.** The mutual diffusion coefficients of the microemulsion droplets were determined by measuring the time-dependent autocorrelation function of the scattered intensity.[55−57] Quasi-elastic Light Scattering (QELS) experiments were carried out on a Brookhaven apparatus (BI 200SM with BI2030AT) by using a coherent argon ion laser ($\lambda = 514$ nm) with a long-term power stability of ±0.5%. The scattered light intensity was detected by an EMI 9863B/350 photomultiplier. A calibration procedure was carried out on a diluted monodisperse suspension of polystirene latex spheres (Serva, 0.06 $\mu$m).

The data were analyzed using the cumulant technique. The autocorrelation function is expanded about an average line width $\Gamma$, as a polynomial in the sample time with cumulants as parameters to be fitted.[58,59] The expansion is stopped to the second-moment result and weighed. The least-squares technique is applied to the second-order polynomial to determine all function constants and their standard deviations.

The average mutual diffusion coefficient $D$, is related to $\Gamma$ by the relation $D = \Gamma/K^2$, where $K = (4\pi n/\lambda)\sin(\theta/2)$ is the scattering wave vector, n the refractive index of the sample and $\theta$ the scattering angle. The deviation of the experimental curve from a single exponential decay is usually given by $\mu_2/\Gamma^2$ (where $\mu_2$ is the second moment of the distribution) and is called "degree of polydispersity".[59] Five millimeter ultraprecision Aldrich NMR premium tubes were used for the experiments. The refraction index of the samples was measured by an Abbe refractometer (Atago 3T) with accuracy better than 0.0002.

**NMR.** $^1$H NMR experiments were performed at 1.88 T on a Varian FT 80A spectrometer at the operating frequency of 80 MHz. The temperature was always kept constant with an accuracy ±0.5 °C.

Diffusion measurements were performed using the Fourier transform pulsed magnetic field gradient spin−echo (FT-PGSE) technique, as described by Stilbs.[60,61] The experiments were carried out by varying the gradient pulse length ($\delta$) while keeping the gradient strength (G) and the pulse interval ($\Delta$) constant. The decay of the echo intensity with increasing the $\delta$ value is given by

$$A(\delta) = A_0 \exp[-D(\gamma\, G\delta)^2(\Delta - \delta/3)]$$

where $D$ is the self-diffusion coefficient, $A_0$ is the echo intensity in the absence of any gradient, and $\gamma$ the magnetogyric ratio.

For $^1$H self-diffusion experiments $\Delta = 70-140$ ms (depending on the water content) and $G = 2$ G/cm were used.

The self-diffusion coefficients were calculated by means of a two-parameter nonlinear fit of the equation above to 10−14 different $\delta$ values. The error in the measurements, as judged by repeated measurements, is estimated to be smaller than ±5%.

## Results and Discussion

**Phase Diagram.** Figure 1A shows the partial phase diagram of CaAOT/water/*n*-decane (CaAOT/W/C10) where the $L_2$ region is evidentiated. The phase boundaries have an accuracy of ±1 wt %. The different liquid and liquid crystalline (LC) regions of the surfactant/water binary system are also shown, but without determining the oil uptake of each phase. The comparison with the corresponding system of the AOT/W/C10 system, redrawn from literature data[13] in Figure 1B, points out the significant shrinkage of the microemulsion region upon substituting the surfactant counterion, similarly to what observed by Khan et al.[46,47] for the $L_\alpha$ phase in the CaAOT/water binary system. The higher $Ca^{2+}$ counterion binding lowers the electrostatic repulsion thus decreasing the swelling capability, which becomes rather significant in the $L_2$ region of the ternary system at high surfactant concentration. It can be suggested that the expected increase of the packing parameter, in terms of "v/al" as defined by Mitchell and Ninham,[62] due to the predominance of the chains' volume of the CaAOT molecule, represents a geometrical constraint which prevents the increase of the mean curvature ($H < 0$) of the surfactant interface. In fact a rather low negative curvature ($H \rightarrow 0$) would be necessary to solubilize larger amounts of water.

The physical properties of the microemulsion region were investigated by several techniques and following various dilution criteria (shown in Figure 1A) with the aim of mapping the microstructural evolutions as a function of composition.

**Viscosity.** Two lines, at the constant water content of 5 and 10 wt %, denoted line 1 and line 2, respectively (see Figure 1A), together with a water dilution line at the surfactant/oil weight ratio s/o = 4/6, denoted line c, were investigated for the viscosity behavior as a function of the volume of the dispersed phase ($\phi_d$). The relative viscosity $\eta_{rel}$ can be expressed according to the following equation:[63]

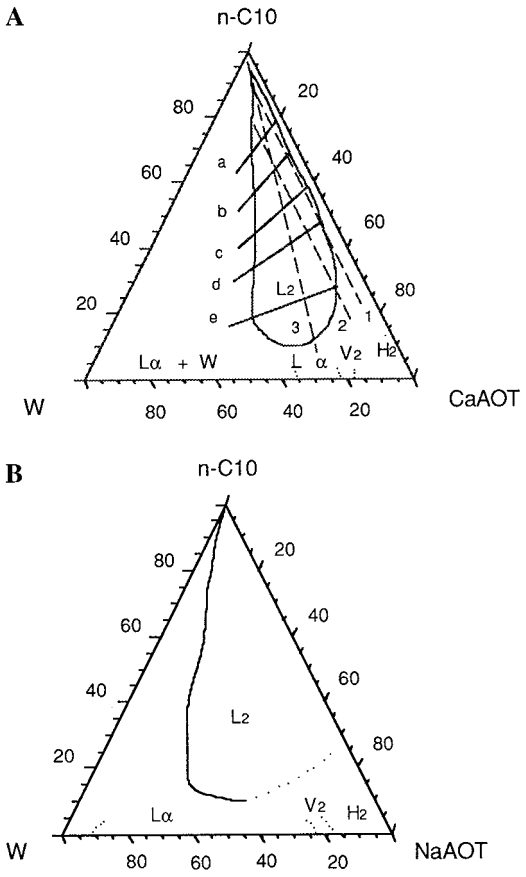


**Figure 1.** (A) Partial phase diagram of CaAOT/W/C10 at 25 °C. Line 1 → at constant 5 wt % water content, line 2 → at constant 10 wt % water content, and line 3 → at costant mass ratio w/s = 35/65 corresponding to the molar ratio w/s = 26.4. Water dilution lines at the constant mass ratios: line a → s/o = 2/8, line b → s/o = 3/7, line c → s/o = 4/6, line d → s/o = 5/5, line e → s/o = 7/3.The phase boundaries on the CaAOT/water binary axis are from ref 46. (B) Partial phase diagram of AOT/W/C10 from refs 13, 46, and 48.

$$\eta_{rel} = \eta/\eta^\circ = 1 + \beta\phi_d + \zeta\phi_d^{\,2} \qquad (1)$$

where $\beta$ is a shape factor and $\zeta$ accounts for interaggregate interactions. With increasing $\phi_d$, at constant water content, $\eta_{rel}$ does not follow eq 1, particularly along line 2 (Figure 2A). This trend suggests deep modifications of the interaggregate interactions and/or microstructural evolutions in terms of size (polidispersity) and shape (deviations from spherical droplets). Along line c (Figure 2B) a maximum is observed at $\phi_d \approx 0.4$, which corresponds to ∼10 wt % of water. This trend recalls that observed for the DDAB/water/*n*-decane system at s/o = 2/8, where a transition from a bicontinuous to a water-in-oil microstructure was found with increasing the water content.[64]

In the $L_2$ region of the ternary AOT/W/C10 system many investigations, based on different experimental techniques, pointed out the occurrence of spherical droplets whose long range order increases with increasing $\phi_d$. Therefore, according to a predominant approach, the starting point for discussing our results concerning CaAOT microemulsions, will consider the spherical model.

**The Spherical Model and the Diffusion Coefficient.** A microstructure of water-in-oil spherical droplets, more or less polydisperse in size and with a variable degree of interaggregate interactions, which depend on composition and temperature, is the most accepted model for AOT w/o microemulsions. Ac-

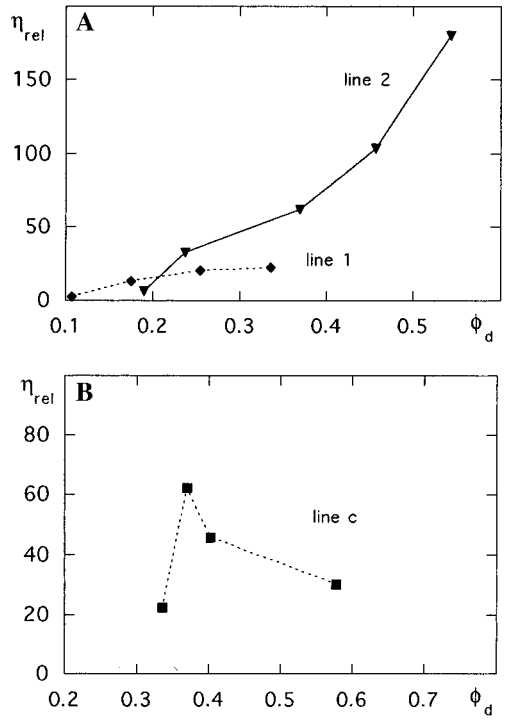


**Figure 2.** Relative viscosity ($\eta_{rel}$) data at 25 °C vs $\phi_d$. (A) (◆) line 1, (▼) line 2, (B) (■) line c.

cording to some authors,[14,65] the radius of the spherical particle depends on the ratio $w°$ between the number of water molecules and that of the surfactant polar heads ($w° = [H_2O]/2[CaAOT]$):

$$R_d\,(\text{nm}) = (3V_w/\sigma)w° + l = 0.175w° + 0.85 \qquad (2)$$

where $V_w = 0.035$ nm$^3$ is the volume of a water molecule, $\sigma = 0.6$ nm$^2$ is the polar head area, and $l = 0.85$ nm is the surfactant chain length, taken as the average between the minimum and the maximum values reported in the literature.

If monodisperse spherical w/o droplets occur in the system, the particle diffusion coefficient due to Brownian motion is given by the Stokes−Einstein equation:

$$D° = kT/6\pi\eta R_d \qquad (3)$$

where $\eta$ is the viscosity of the medium ($\eta_{dec} = 0.838$ cP for decane at 25 °C). This law is rigorously valid at infinite dilution only. In fact, the diffusion coefficient changes with increasing $\phi_d$ due to particle interactions, and, for our experimental techniques (NMR spin−echo or DLS), can be expressed as[66,67]

$$D_{NMR,DLS} = D°(1 + \alpha\phi_d) \qquad (4)$$

where $D_{NMR}$ represents a translational self-diffusion coefficient measured over a long time scale (0.1 s), and $D_{DLS}$ represents a collective diffusion coefficient,[66,68] obtained over a much shorter time scale ($10^{-6}$ s) from the fit of the correlation function of the scattered light. For diluted systems, taking only pairwise hydrodynamic interactions into account, $\alpha_{DLS} = 1.45-1.56$ and $\alpha_{NMR} = -2$ [66,68] generally apply for the collective and for the long time diffusion coefficients respectively, within the hard sphere model approximation.

**Dynamic Light Scattering (DLS) Measurements.** The diffusion coefficients, obtained from DLS measurements for the same samples investigated by viscosity, do not depend on the scattering angle appreciably, and are reported in Figure 3A for

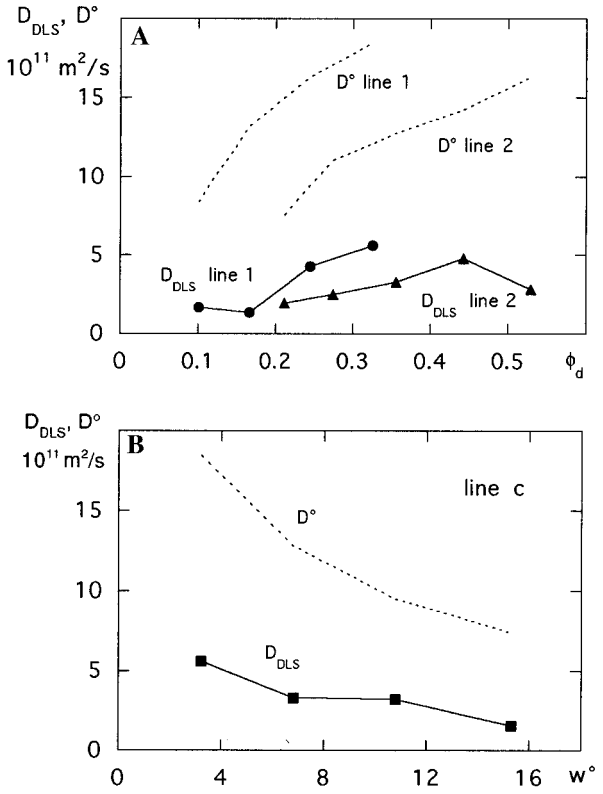


**Figure 3.** Diffusion coefficient $D_{DLS}$ from DLS measurements at 25 °C and calculated $D°$ (dashed lines) from composition by eqs 2−3. (A) vs $\phi_d$ line 1 (●) exp., line 2 (▲) exp. (B) vs $w°$ line c (■) exp.

line 1 and 2, as a function of $\phi_d$, and in Figure 3B for line c, as a function of $w°$. The corresponding $D°$ values, calculated from composition by eqs 2 and 3, are also shown.

The hard sphere model obviously does not interpret the data properly, since $D° \gg D_{DLS}$ is always observed. With increasing $\phi_d$, polydispersity, obtained by the relative variance from the cumulant fits of DLS data, increases slightly, and thus cannot, alone, account for the observed discrepancies. Indeed the occurrence of nonspherical shape droplets and of cluster structures or more complex aggregates, whose extent increases with increasing $\phi_d$, is likely to play a major role. A prolate or oblate particle introduces a correction factor which decreases the observed diffusion coefficient.[69] However, the occurrence of important deviations from a hard-sphere interaction model of the microstructure can be directly inferred either by considering the $\alpha_{DLS}$ calculated from the $D_{DLS}/D°$ ratios or by calculating the correlation length $\xi = kT/6\pi\eta D_{DLS}$.[25] These data are shown in Table 1. The always negative $\alpha_{DLS}$ values and the $\xi$ values significantly higher than $R_d$ suggest the occurrence of strongly interacting particles whose average shape cannot be spherical over the DLS observation time scale.

The hard sphere w/o droplet model is likely to fit the experimental data at very low $\phi_d$ values, only. The $D_{DLS}$ diffusion coefficient is extremely sensitive to interdroplet interactions, hence it can be related to the existence of spherical droplets, without any doubt, only at $\phi_d \to 0$, or at least when interdroplet attractive interactions can be reasonably neglected.

**NMR Self-Diffusion Measurements.** The NMR self-diffusion measurements are very sensitive to the dimensions of the microdomains over which molecules can move, during a defined observation time $t$, according to Einstein relation:

$$\langle x\rangle = (6Dt)^{0.5} \qquad (5)$$

where $\langle x\rangle$ is the mean free path and $D$ the self-diffusion

**TABLE 1: Experimental $D_{DLS}$ and $D_{NMR}$ Diffusion Coefficients along Line 1, Line 2, and Line C, Compared with $R_d$ and $D°$ Values Obtained from Composition[a]**

| $\phi_d$ | $R_d$, nm | $D°$, $10^{11}$ m$^2$/s | $D_{DLS}$, $10^{11}$ m$^2$/s | $\alpha_{DLS}$ | $\zeta$, nm | $D_{NMR}$,[a] $10^{11}$ m$^2$/s | $\alpha_{NMR}$ |
|---|---|---|---|---|---|---|---|
| line 1 | | | | | | | |
| 0.101 | 3.10 | 8.40 | 1.66 | −7.94 | 15.69 | | |
| 0.167 | 1.97 | 13.22 | 1.33 | −5.39 | 19.51 | | |
| 0.245 | 1.60 | 16.28 | 4.24 | −3.02 | 6.14 | | |
| 0.326 | 1.41 | 18.47 | 5.59 | −2.14 | 4.66 | | |
| line 2 | | | | | | | |
| 0.212 | 3.45 | 7.55 | 1.93 | −3.51 | 13.50 | 4.43 | −1.94 |
| 0.275 | 2.35 | 11.08 | 2.48 | −2.82 | 10.50 | 8.60 | −0.81 |
| 0.356 | 2.04 | 12.77 | 3.29 | −2.08 | 7.92 | 8.59 | −0.92 |
| 0.443 | 1.83 | 14.23 | 4.76 | −1.50 | 5.47 | 3.75 | −1.66 |
| 0.530 | 1.60 | 16.28 | 2.84 | −1.56 | 9.17 | 3.29 | −1.51 |
| 0.665 | 1.55 | 16.76 | | | | 1.56 | −1.36 |
| line 3 | | | | | | | |
| 0.326 | 1.41 | 18.47 | 5.59 | −2.14 | 4.66 | | |
| 0.356 | 2.04 | 12.77 | 3.29 | −2.08 | 7.92 | 8.59 | −0.92 |
| 0.387 | 2.74 | 9.51 | 3.20 | −1.71 | 8.13 | 13.10 | 0.98 |
| 0.419 | 3.53 | 7.38 | 1.53 | −1.89 | 17.02 | 11.02 | 1.18 |

[a] Calculated assial ratio for prolate and oblate shape of the droplets, obstruction values $\alpha_{DLS}$ and correlation length $\zeta$ from experimental $D_{DLS}$. Calculated obstruction values $\alpha_{NMR}$ from experimental $D_{NMR}$. $R_d$ from eq 2; $D°$ from eq 3; $\alpha_{DLS}$ from eq 4; $\zeta = kT/6\pi\eta D_{DLS}$; $\alpha_{NMR}$ from eq 4 [b] The low amount of water prevented water self-diffusion measurements along line 1.

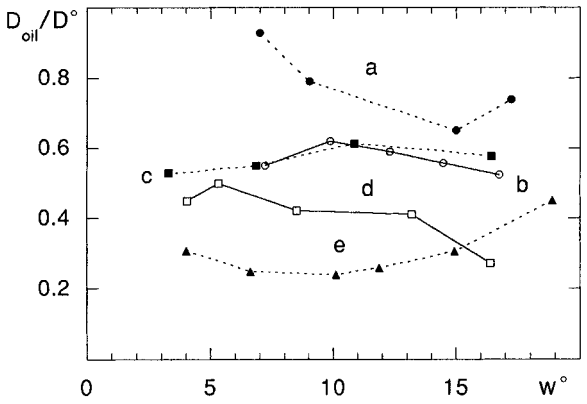


**Figure 4.** Reduced oil self-diffusion coefficients $D_{oil}/D°$ at 25 °C, where $D° = 1.38\ 10^{-9}$ m$^2$/s for *n*-decane at 25 °C.[74] $D_{oil}/D°$ vs $w°$ for the water dilution lines: (●) line a; (○) line b; (■) line c; (□) line d; (▲) line e.

coefficient. For a molecular species moving within a continuous medium, such as the oil molecules of our microemulsions, diffusion is unrestricted and the observed self-diffusion coefficient $D_{oil}$ is always high, at most it can be slightly reduced when the volume fraction of the dispersed phase increases significantly (i.e. $\phi_d > 0.7$). In our system, independently on the organization of the hydrophilic domain, the oil self-diffusion data, shown in Figure 4 for the water dilution lines a−e, confirm that oil is always a continuous phase and its motion is not seriously affected by the increase of $\phi_d$.

In the case of molecular species confined in restricted domains, such as the water molecules inside a droplet, it has been demonstrated that the self-diffusion coefficient $D_w$ is predominantely determined by the Brownian motion of the droplet. Thus $D_w \approx D_{NMR}$. Obviously the effective motion is strictly related to the size and shape of the particle besides the nature of the medium. For hard sphere droplets eq 4 holds, while, as a result of the occurrence of nonspherical particles, a decrease of the measured self-diffusion coefficient is expected also for $D_{NMR}$. A further decrease of $D_w$ may arise from tightly bound water molecules, such as hydration water, for which a decrease of about 1 order of magnitude has been suggested. This effect, however, is evident only at water/surfactant molar ratio smaller than 4−5.

The NMR experiments were performed along line 2 and several water dilution lines at fixed s/o mass ratio, namely s/o = 2/8 (line a), s/o = 3/7 (line b), s/o = 4/6 (line c), s/o = 5/5 (line d), and s/o = 7/3 (line e).

Before discussing NMR data in details, it seems of interest to compare DLS and NMR data. As shown in Table 1 for line 2 and line c, the self-diffusion coefficients $D_w = D_{NMR}$ are rather different from $D_{DLS}$, except at high $\phi_d$, with generally $D_{NMR} > D_{DLS}$. It should be noted that along line c $D_{NMR}$ exceedes $D°$. Indeed, from the $D_{NMR}/D°$ ratios $\alpha < 2$ values are obtained for line 2, whereas for line c, $\alpha$ becomes positive. It is evident that the hard sphere model must be ruled out also on the basis of NMR $D_w$. It should be noticed that NMR data give evidence of important hydrodynamic interactions which can be justified by the presence of a "water continuous network". The appearance of a long water path may be due either to a real bicontinuous microstructure or to strong attractive interdroplet interactions which occur on the same time scale of the experimental observation. Indeed NMR spin−echo time scale is about 6 orders of magnitude larger than DLS observation time.

Figure 5A reports the reduced self-diffusion coefficients $D_w/D_w°$ (where $D_w° = 2.29 \times 10^{-9}$ m$^2$/s, is the pure water self-diffusion constant at 25 °C[70]) for the various water dilution lines as a function of $w°$. The hard sphere model of eq 4 ($\alpha = -2$) agrees with the experimental $D_w/D_w°$ only along line a (Figure 5B), where the lowest values of $\phi_d$ (0.17−0.23) are considered. For the other water dilution lines $D_w/D_w°$ does not show a monotonic trend, and a maximum, whose relative value increases with increasing the s/o ratio, appears in the range $10 < w° < 19$. This trend is very different from what one would expect in the presence of defined particles which increase in size with increasing $w°$, and is indicative of deep structural modifications as far as the water domain concerns.

**Conductivity along the Water Dilution Lines.** Figure 5C shows the conductivity data collected at 25 °C along the various water dilution lines and reported as a function of $w°$. The various curves display a clear maximum of conductivity which occurs from $w° \approx 7.5$ for line a to $w° \approx 10.7$ for line e. The conductivity for line e does not decrease significantly with increasing $w°$ up to the phase boundary which occurs at $w° \approx 20$. The range of high conductivity enlarges and flattens, while its absolute value increases, with increasing the s/o ratio. It is evident that conductivity data (Figure 5C) parallel very closely the NMR self-diffusion coefficients (Figure 5A), since the two experimental techniques sample the transport properties of the system over comparable time scales.

It is worth noticing the striking similarities between these trends and those observed for other w/o microemulsions, for which conductivity and self-diffusion data were interpreted in terms of the geometrical DOC model.[44] In that case the conducting-nonconducting transition (time dependent static percolation threshold[71]) was observed at a degree of connectivity $Z \approx 1.3$.

**Conductivity and Percolative Behavior.** As widely demonstrated in the literature, a strong attractive interdroplet interaction scheme can be rationalized in terms of static or dynamic percolation phenomena. Besides kinetic considerations, temperature and composition (which settles size and shape of the aggregates) must be considered as the most crucial factors to determine the percolation threshold. For instance,

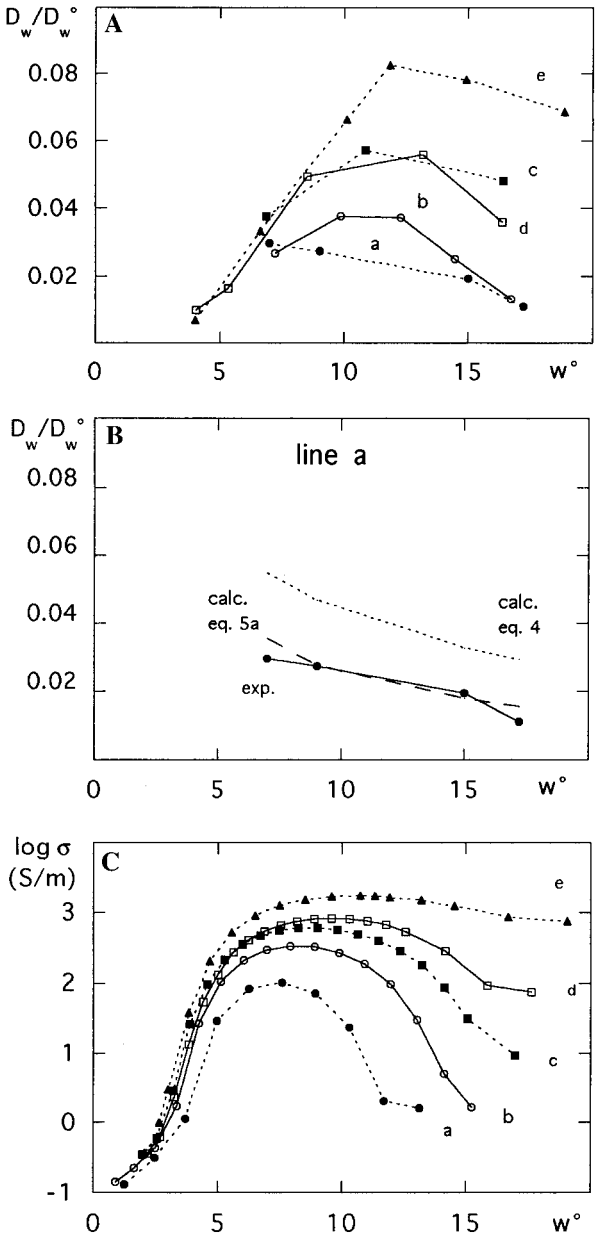


**Figure 5.** NMR $D_w/D_w°$ data and conductivity (log $\sigma$) vs $w°$ at 25 °C along the various water dilution lines: (●) line a; (○) line b; (■) line c; (□) line d; (▲) line e. (A) $D_w/D_w°$ vs $w°$; $D° = 2.29 \times 10^{-9}$ m²/s is the pure water self-diffusion coefficient at 25 °C.[70] (B) (l) Line a and the corresponding values calculated by eq 3 (···) and by eq 4 (- - -) with $\alpha = -2$. (C) log $\sigma$ vs $w°$.

for the $L_2$ region of the AOT/W/C10 system, 25 °C is a transition temperature in a large range of composition.[30]

To investigate the structural changes induced by percolation phenomena, an oil dilution line at the molar ratio w/s = 26.4 (line 3, at the water/surfactant mass ratio 35/65, in Figure 1A), which crosses the middle range of the $L_2$ region, was investigated by conductivity at 15, 25, and 30 °C. The conductivity does not depend on the temperature significantly, and displays a sharp increase of about 4 orders of magnitude with increasing $\phi_d$, as shown in Figure 6A. The occurrence of a percolative phenomenon is rather obvious at the critical volume fraction of the dispersed phase $\phi_d^c \approx 0.140-0.145$. The absence of a temperature dependence suggests the possibility of a microstructural evolution which is dependent on the composition only, that means a static rather than a dynamic percolative process, at least in the range of temperature 15−30 °C. It is worth noticing that introducing our $\phi_d^c = 0.1425$ into the typical

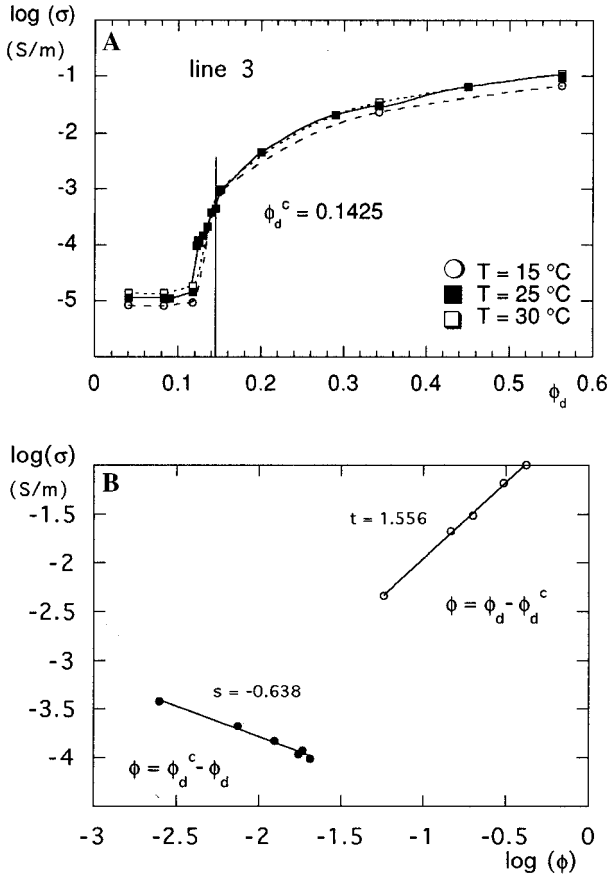


**Figure 6.** (A) Conductivity (log $\sigma$) vs $\phi_d$ at 3 different temperatures for line 3, (○) $T = 15$ °C, (■) $T = 25$ °C, (□) $T = 30$ °C. The percolation threshold is indicated at the critical $\phi_d^c \sim 0.1425$ and is not dependent on temperature. (B) Calculation of the indices "s" and "t", below and above the percolation threshold, respectively.

equations:[37]

$$\sigma \approx (\phi_d^c - \phi_d)^{-s} \quad \text{at } \phi_d < \phi_d^c$$

(below percolation threshold) (6a)

$$\sigma \approx (\phi_d - \phi_d^c)^t \quad \text{at } \phi_d > \phi_d^c$$

(above percolation threshold) (6b)

we obtain, from data at 25 °C, the critical exponents $s = 0.636$ and $t = 1.556$, as shown in Figure 6B. These values are close with those reported ($s = 0.7$ and $t = 1.9$) for microemulsions undergoing static percolative processes.[37,72] In the case of AOT/W/C10 microemulsions,[33] from the temperature dependence of the conductivity of a sample at w/s = 26.3, $s \approx 1.2$, and $t = 1.86$ were calculated, in agreement with a dynamic percolation model.[37] The value $\phi_d^c \approx 0.14$ agrees with data reported also by Jada et al.[40] for AOT w/o microemulsions. Such a value of $\phi_d$ is needed to increase the attractive interactions among the droplets thus favoring the exchange of material. As a consequence of this exchange, conductivity and water self-diffusion increase.

The observation that transport parameters do not show a monotonic trend along the various b−e dilution lines can be interpreted in terms of fusion−fission processes among the droplets for which the time scale of the interaction strongly depends on the size. The closed particle structure displays "transient" interparticle connections which mimic a water continuous network as far as molecular transport concerns, provided that the time scale of the interaction is comparable with the observation time. Through the Einstein equation, eq

5, it is easy to determine the path available for a molecular diffusion ranging between $10^{-12}$ and $10^{-9}$ $m^2/s$. $D_w$ values ranging around $10^{-10}$ $m^2/s$ are indicative of still large domains available for water motions, and are typical of water continuous networks.[45] This suggestion is strongly supported by a direct comparison between water self-diffusion data (observation at a molecular level) and the trend of conductivity (observation of the macroscopic ion transport) measured along the various water dilution lines.

### Concluding Remarks on the Microstructure

Nonspherical shapes of the particles, polidispersity and interdroplet attractive interactions can play a crucial role in determining the effective Brownian motion in microemulsions.

The choice of a suitable model to interpret the structural features of a highly dynamic system such as a microemulsion depends on the time scale of the experimental observation. In terms of percolation theory, the conductivity indices along the oil dilution line suggest the occurrence of a static percolation. In addition, the conductivity trend does not depend on temperature significantly, at least in the range 15−30 °C. However, it is worth noting that the attempt to discriminate between dynamic and static percolation is likely to be a rather restrictive viewpoint. In the case of several DDAB and PFPE w/o microemulsions[43,44] the experimental conductivities and diffusion data, interpreted in terms of the DOC model, pointed out a gradual evolution of the microstructure from bicontinuity (at low water content) to disconnected w/o droplets (at high water content). By analogy, a transition from a connected water network to closed water domains through a gradual variation of the connectivity Z can be hypothesized for CaAOT/W/C10 w/o microemulsions. In addition, the observation that along line d and line e, and differently from the line b and line c, both conductivity and NMR self-diffusion coefficients give rather high values even at large $w°$ values, in the vicinity of the phase boundary, suggests the presence of a water network still partially connected as observed for a PFPE microemulsion. In that case this behavior was ascribed to the use of a low penetrating PFPE oil with a much higher MW than the PFPE surfactant. Similar behavior was observed also for DDAB with the tetradecane oil.[73] For CaAOT microemulsions, due to surfactant packing constraints at high surfactant concentration, the formation of disconnected droplets, which would have a too high inverse curvature of the surfactant interface (because of the low amount of water), is not allowed.

**Acknowledgment.** M.M. thanks B.W. Ninham and S. Hyde for stimulating discussions. MURST (Italy), CNR (Italy), Consorzio Sistemi Grande Interfase (CSGI−Firenze), and Assessorato Igiene Sanita' (Sardinia Region-Cagliari) are acknowledged for support.

### References and Notes

(1) Eicke, H. F.; Rehak, J. *Helv. Chim. Acta* **1976**, *59*, 2883−2891.
(2) Eicke, H. F. *Top. Curr. Chem.* **1980**, *87*, 85.
(3) Luisi, P. L.; Magid, L. *Crit. Rev. Biochem.* **1986**, *20*, 409 and references therein.
(4) Luisi, P. L.; Giomini, M.; Pileni, M. P.; Robinson, B. H. *Biochem. Biophys. Acta* **1988**, *947*, 209 and references therein.
(5) Eicke, H. F.; Hilfiker, R.; Holz, M. *Helv. Chim. Acta* **1984**, *67*, 361.
(6) Eicke, H. F.; Borkovec, M.; Das-Gupta, B. *J. Phys. Chem.* **1989**, *93*, 4.
(7) Fletcher, P. D. I.; Howe, A. M.; Robinson, B. H. *J. Chem. Soc., Faraday Trans.* **1987**, *83*, 985−1006.
(8) Lang, J.; Jada, A.; Malliaris, A. *J. Phys. Chem.* **1988**, *92*, 1946.
(9) Dijk, M. A. v.; Joosten, J. G. H.; Levine, Y. K.; Bedeaux, D. *J. Phys. Chem.* **1989**, *93*, 2506.
(10) Robertus, C.; Joosten, J. G. H.; Levine, Y. K. *Phys. Rev. A* **1990**, *42*, 4820.
(11) Zulauf, M.; Eicke, H.-F. *J. Phys. Chem.* **1979**, *83*, 480.
(12) Robinson, B. H.; Toprakcioglu, C.; Dore, J. C.; Chieux, P. *J. Chem. Soc., Faraday Trans. 1* **1984**, *80*, 13.
(13) Kotlarchyk, M.; Chen, S. H.; Huang, J. S.; Kim, M. W. *Phys. Rev. A* **1984**, *29*, 2054.
(14) Pileni, M. P.; Zemb, T.; Petit, C. *Chem. Phys. Lett.* **1985**, *118*, 414−420.
(15) Kotlarchyk, M.; Stephens, R. B.; Huang, J. S. *J. Phys. Chem.* **1988**, *92*, 1533.
(16) DeMarco, A.; Menegatti, E.; Luisi, P. L. *J. Biochem. Biophys. Meth.* **1986**, *12*, 325−333.
(17) Carnali, J.; Lindman, B.; Soderman, O.; Walderhaug, H. *Langmuir* **1986**, *2*, 51.
(18) Carnali, J. O.; Ceglie, A.; B.Lindman; Shinoda, K. *Langmuir* **1986**, *2*, 417.
(19) Geiger, S.; Eicke, H.-F. *J. Colloid Interface Sci.* **1986**, *110*, 181.
(20) Carlstrom, G.; Halle, B. *Langmuir* **1988**, *6*, 1346−1352.
(21) Carlstrom, G.; Halle, B. *J. Phys. Chem.* **1989**, *93*, 3287−3299.
(22) Furo′, I.; Halle, B.; Quist, P.; Wang, T. C. *J. Phys. Chem.* **1990**, *94*, 2600−2613.
(23) Martinek, J. *Eur. J. Biochem.* **1986**, *155*, 453.
(24) Huang, J. S. *J. Surf. Sci. Technol.* **1989**, *5*, 83.
(25) Eastoe, J.; Robinson, B. H.; Steytler, D. C.; Thorn-Leeson, D. *J. Colloid Interface Sci.* **1991**, *36*, 1−31.
(26) Kotlarchyk, M.; Sheu, E. Y.; Capel, M. *Phys. Rev. A* **1992**, *46*, 928.
(27) Yoshino, A.; Okabayashi, H.; Yoshida, T. *J. Phys. Chem.* **1994**, *98*, 7036.
(28) Kurumada, K.; Shioi, A.; Harada, M. *J. Phys. Chem.* **1994**, *98*, 12382.
(29) Kurumada, K.; Shioi, A.; Harada, M. *J. Phys. Chem.* **1995**, *99*, 16982.
(30) Feldman, Y.; Kozlovich, N.; Nir, I.; Garti, N. *Phys. Rew. E* **1995**, *51*, 478, and references therein.
(31) Bardez, E.; Vy, N. C.; Zemb, T. *Langmuir* **1995**, *11*, 3374.
(32) Berghenholtz, J.; Romagnoli, A.; Wagner, N. *Langmuir* **1995**, *11*, 1559.
(33) Feldman, Y.; Kozlovich, N.; Nir, I.; Garti, N.; Archpov, V.; Idiyatullin, Z.; Zuev, Y.; Fedotov, V. *J. Phys. Chem.* **1996**, *100*, 3745.
(34) Jahn, W.; Strey, R. *J. Phys. Chem.* **1988**, *92*, 2294.
(35) Cametti, C.; Codastefano, P.; Tartaglia, P.; Chen, S. H.; Rouch, J. *Phys. Rev. A* **1992**, *45*, 5359, and references therein.
(36) Kotlarchyk, M.; Chen, S. H.; Huang, J. S.; Kim, M. W. *Phys. Rev. Lett.* **1984**, *53*, 941.
(37) Ponton, A.; Bose, T. K.; Delbos, G. *J. Chem. Phys.* **1991**, *94*, 6879.
(38) deGennes, P. G.; Taupin, C. *J. Phys. Chem.* **1982**, *86*, 2294.
(39) Grest, G.; Webman, I.; Safran, S.; Bug, A. *Phys. Rev. A* **1986**, *33*, 2842.
(40) Jada, A.; Lang, J.; Zana, R. *J. Phys. Chem.* **1989**, *93*, 10.
(41) Hyde, S. T. *J. Phys. Chem.* **1989**, *93*, 1458.
(42) Hyde, S. T.; Ninham, B. W.; Zemb, T. *J. Phys. Chem.* **1989**, *93*, 1464.
(43) Knackstedt, M. A.; Ninham, B. W. *Phys. Rev. E* **1994**, *50*, 2839, and reference therein.
(44) Monduzzi, M.; Knackstedt, M. A.; Ninham, B. W. *J. Phys. Chem.* **1995**, *99*, 17772.
(45) Guering, P.; Lindman, B. *Langmuir* **1985**, *1*, 464.
(46) Khan, A.; Fontell, K.; Lindman, B. *J. Colloid Interface Sci.* **1984**, *101*, 193.
(47) Khan, A.; Jönsson, B.; Wennerström, H. *J. Phys. Chem.* **1985**, *89*, 5180.
(48) Franses, E. I.; Hart, T. J. *J. Colloid Interface Sci.* **1983**, *94*, 1−13.
(49) Kandori, K.; Kon-no, K.; Kitahara, A. *J. Colloid Interface Sci.* **1988**, *122*, 78.
(50) Bardez, E.; Larrey, B.; Zhu, X. X.; Valeur, B. *Chem. Phys. Lett.* **1990**, *171*, 362.
(51) Eastoe, J.; Fragneto, G.; Robinson, B. H.; Towey, T. F.; Heenan, R. K.; Leng, F. J. *J. Chem. Soc., Faraday Trans.* **1992**, *88*, 461−471.
(52) Eastoe, J.; Towey, T. F.; Robinson, B. H.; Williams, J.; Heenan, R. K. *J. Phys. Chem.* **1993**, *97*, 1459.
(53) Giordano, R.; Migliardo, P.; Wanderlingh, U.; Bardez, E. *J. Mol. Struct.* **1993**, *296*, 265.
(54) Petit, C.; Lixon, P.; Pileni, M. P. *Langmuir* **1991**, *7*, 2620.
(55) Chu, B. *Laser Light Scattering*; Academic Press: New York, 1974; p 185.
(56) Berne, B. J.; Pecora, R. *Dinamic Light Scattering with Application to Chemistry, Biology and Physics*; Wiley-Interscience: New York, 1976.
(57) Pecora, R. *Dinamic Light Scattering: Application of Photon Correlation Spectroscopy*; Plenum: New York, 1985.
(58) Koppel, D. E. *J. Chem. Phys.* **1972**, *57*, 4814−20.
(59) Brown, J. C.; Pusey, P. N.; Dietz, R. *J. Chem. Phys.* **1975**, *62*, 1136−44.
(60) Stejskal, E. O.; Tanner, J. E. *J. Chem. Phys.* **1965**, *42*, 288.

(61) Stilbs, P. *Prog. NMR Specrosc.* **1987**, *19*, 1, and reference therein.
(62) Mitchell, D. J.; Ninham, B. W. *J. Chem. Soc., Faraday Trans. 2* **1981**, *77*, 601.
(63) Frish, H. L.; Simha, R. In *Rheology*; F. R. Eirich, Ed.; Academic Press: New York, 1956; Vol. 1.
(64) Chen, S. J.; Evans, D. F.; Ninham, B. W.; Mitchell, D. J.; Blum, F. D.; Pickup, S. *J. Phys. Chem.* **1986**, *90*, 842−847.
(65) Kotlarchyk, M.; Chen, S. H.; Huang, J. S. *J. Phys. Chem.* **1982**, *86*, 3273−76.
(66) Ohtsuki, T.; Okano, K. *J. Chem. Phys.* **1982**, *77*, 1443.
(67) Lekkerkerker, H. N. W.; Dhont, J. K. G. *J. Chem. Phys.* **1984**, *80*, 5790.
(68) Olsson, U.; Schurtenberger, P. *Langmuir* **1993**, *9*, 3389.
(69) Balinov, B.; Olsson, U.; Soderman, O. *J. Phys. Chem.* **1991**, *95*, 5931.
(70) Mills, R. *J. Phys. Chem.* **1973**, *77*, 685.
(71) Knackstedt, M. A.; Ninham, B. W.; Monduzzi, M. *Phys. Rev. Lett.* **1995**, *75*, 653.
(72) deGennes, P. G. *J. Phys. (Paris)* **1980**, *41*, C13.
(73) Monduzzi, M.; Caboi, F.; Larche′, F.; Olsson, U. *Langmuir* **1997**, *13*, 2184.
(74) Ertl, H.; Dullien, F. A. L. *AIChE J.* **1973**, *19*, 1215.